Available online at www.sciencedirect.com
ScienceDirect
Science of the Total Environment 381 (2007) 263–279
Science of the Total Environment
An International Journal for Scientific Research into the Environment and its Relationship with Humankind
www.elsevier.com/locate/scitotenv

Geochemistry of trace metals in a fresh water sediment: Field results and diagenetic modeling

R.W. Canavan [a,*], P. Van Cappellen [a], J.J.G. Zwolsman [b], G.A. van den Berg [b], C.P. Slomp [a]

[a] *Utrecht University, Faculty of Geosciences, PO Box 80021, 3508 TA Utrecht, The Netherlands*
[b] *Kiwa Water Research, PO Box 1072, 3430 BB Nieuwegein, The Netherlands*

Received 6 October 2006; received in revised form 27 February 2007; accepted 1 April 2007
Available online 4 May 2007

Abstract

Concentrations of Fe, Mn, Cd, Co, Ni, Pb, and Zn were determined in pore water and sediment of a coastal fresh water lake (Haringvliet Lake, The Netherlands). Elevated sediment trace metal concentrations reflect anthropogenic inputs from the Rhine and Meuse Rivers. Pore water and sediment analyses, together with thermodynamic calculations, indicate a shift in trace metal speciation from oxide-bound to sulfide-bound over the upper 20 cm of the sediment. Concentrations of reducible Fe and Mn decline with increasing depth, but do not reach zero values at 20 cm depth. The reducible phases are relatively more important for the binding of Co, Ni, and Zn than for Pb and Cd. Pore waters exhibit supersaturation with respect to Zn, Pb, Co, and Cd monosulfides, while significant fractions of Ni and Co are bound to pyrite. A multi-component, diagenetic model developed for organic matter degradation was expanded to include Zn and Ni dynamics. Pore water transport of trace metals is primarily diffusive, with a lesser contribution of bioirrigation. Reactions affecting trace metal mobility near the sediment–water interface, especially sulfide oxidation and sorption to newly formed oxides, strongly influence the modeled estimates of the diffusive effluxes to the overlying water. Model results imply less efficient sediment retention of Ni than Zn. Sensitivity analyses show that increased bioturbation and sulfate availability, which are expected upon restoration of estuarine conditions in the lake, should increase the sulfide bound fractions of Zn and Ni in the sediments.

Keywords: Rhine–Meuse River Delta; Sulfide; Trace metals; Diagenetic modeling; Sediment

1. Introduction

Elevated concentrations of trace metals in sediments pose toxicological risks to biota and may impair water quality (Baird and Cann, 2005). Under oxidizing conditions, trace metals bind to organic matter (OM), clays, and Fe plus Mn-oxides (Turner et al., 2004). These phases are frequently intimately associated with one another (Perret et al., 2000; Taillefert et al., 2002), making it difficult to separate them by physical and chemical techniques. Decomposition of OM and reductive dissolution of Fe and Mn-oxides, which tend to be highest near the sediment water interface (SWI; Canavan et al., 2006; Douglas and Adeney, 2000), may lead to release of trace metals to the pore waters (Zhang et al., 1995).

In reducing sediments, trace metals often associate with insoluble sulfide precipitates (e.g. Huerta-Diaz et al., 1998). Sulfide is produced by bacterial sulfate reduction coupled to OM decomposition (Holmer and Storkholm,

* Corresponding author. Tel.: +31 302535016; fax: +31 302535302.
E-mail address: r.canavan@geo.uu.nl (R.W. Canavan).

0048-9697/$ - see front matter © 2007 Elsevier B.V. All rights reserved.
doi:10.1016/j.scitotenv.2007.04.001

2001). In coastal marine sediments and salt marsh soils, abundant sulfate and OM cause high rates of sulfide production, with pyrite (FeS_2) being the most common end-product (Huerta-Diaz and Morse, 1990; Kostka and Luther, 1994). In freshwater sediments, sulfide mineral phases may also immobilize trace metals, despite the lower sulfate concentrations relative to marine systems (Huerta-Diaz et al., 1998; Motelica-Heino et al., 2003). The metals are then buried in the sediment, unless oxidative dissolution of the sulfide mineral phases occurs, upon sediment mixing by resuspension and bioturbation (Carroll et al., 2002).

Reactive transport models (RTMs) are often used to simulate the complex interplay of reaction and transport processes in sediments (Boudreau, 1999). However, only few studies have used this approach to quantitatively describe trace metal cycling in freshwater sediments. Recently, Gallon et al. (2004) used an inverse, steady state model to describe Pb diagenesis in sediments of a Canadian shield lake. Others have applied multi-component RTMs to assess metal sulfide oxidation (Carbonaro et al., 2005; Di Toro et al., 1996) and the controls on arsenic mobility in sediments (Smith and Jaffe, 1998).

In this study, we present results of pore water analyses and sediment extractions for Fe, Mn, Cd, Co, Ni, Pb and Zn in sediment of a coastal fresh water lake, Haringvliet Lake, which is part of the Rhine–Meuse River Delta and has experienced elevated trace metal inputs from anthropogenic sources. We also include Zn and Ni in an existing multi-component RTM, which accounts for organic matter degradation, secondary redox reactions, mineral precipitation and dissolution, and transport by bioirrigation and bioturbation (Canavan et al., 2006). The analytical results, thermodynamic calculations, and reactive transport modeling are used to examine how trace metal speciation changes with depth in the sediment. A better understanding of trace metal behavior in sediments is needed to guide management efforts to improve water quality and ecosystem health of the lake.

2. Study site

In 1970, the Haringvliet estuary was converted to a freshwater lake by building a dam at the outlet to the North Sea (Fig. 1). This alteration caused the accumulation of metal-polluted sediments in the lake and habitat loss (Smit et al., 1997). A partial restoration of estuarine conditions is proposed for Haringvliet Lake, beginning in 2008. Changes in management of the dam will allow water from the adjacent North Sea to enter the lake at high tide. The sampling site lies within the area that will be affected by the estuarine restoration (Fig. 1; 51.50.080 N, 04.04.328 E).

Trace metal contamination has adversely affected benthic communities in sediments of the Rhine–Meuse Delta where low species diversity has been correlated with sediment toxicity including elevated trace metal

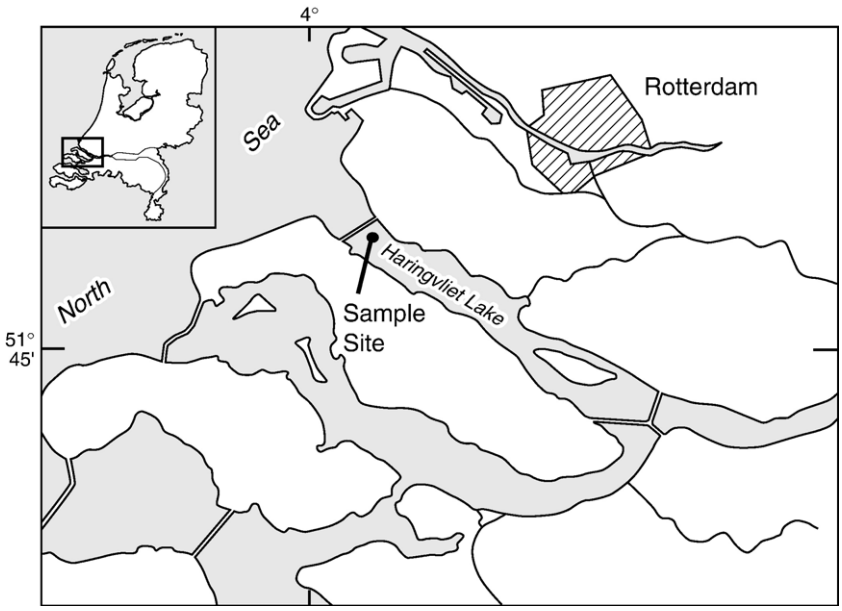

Fig. 1. The sampling location in Haringvliet Lake. The inset map shows the Netherlands with a box denoting the location of the detail section. The Rhine–Meuse river complex flows into the lake from the east, and the lake discharges through the dam at the western limit of the lake.

concentrations (Reinhold-Dudok van Heel and den Besten, 1999). Studies of sediment trace metal biogeochemistry, including pore water analysis, have been conducted at other locations within the delta with the aim of describing possible release of trace metals from the sediment to the overlying water (van den Berg et al., 1999). The present work is part of a study of biogeochemical processes and their response to salinization in Haringvliet Lake.

3. Methods

3.1. Sample collection

Sediment and pore water samples were collected in September 2002, and April–May 2003. The sampling periods are referred to as late-summer, and spring, respectively. Sediment was collected using a cylindrical box corer, with a 31 cm inner diameter, deployed from RV Navicula. Each box core contained approximately 40 cm of surface sediment and 30 cm of overlying water. Sub-cores were taken with polycarbonate tubes (10 cm i.d.). Sub-cores for pore water and solid phase analysis were taken from a single box core and immediately sectioned in a N_2 purged glove box on board the ship.

3.2. Pore water analyses

Sediment sub-samples for pore water collection were placed in polyethylene centrifuge tubes in a N_2 purged glove box during core sectioning. The tubes were subsequently removed from the glove box and centrifuged at 2500 g for 10 to 30 min. Core sectioning and centrifugation were conducted in the temperature controlled laboratory on board with the temperature set to the bottom water temperature during sampling (18 °C late-summer, 12 °C spring). Following centrifugation, tubes were transferred to a N_2 filled glove bag where pore water was filtered (late-summer: 0.2 μm pore size polypropylene PALL filters; spring: 0.45 μm pore size polyethersulfone Orange Scientific filters). Pore water pH was determined directly on the filtrate. Filtrate aliquots for trace metal analysis were acidified with HNO_3 (50 μl conc. trace metal grade HNO_3 per ml) and stored in high density polyethylene bottles at 4 °C until analysis by inductively coupled plasma mass spectroscopy (ICP-MS; Agilent 7500 series). Pore water blanks were determined by processing ultra-pure water from the laboratory in parallel with pore water samples in the field.

Sulfate and chloride were determined by Ion Chromatography (Dionex DX-120) on frozen filtrate, and dissolved organic carbon (DOC) with a Shimadzu TOC-50550A analyzer on filtrate samples stored at 4 °C. Alkalinity was determined colorimeterically in the field (Sarazin et al., 1999). Sulfide was measured colorimeterically (Cline, 1969) using filtered pore water fixed with NaOH (10 μl 1 M NaOH per ml). Sulfide pore water profiles were also measured using the Diffusive Gradient in Thin Films (DGT) method (Motelica-Heino et al., 2003; Naylor et al., 2004). Briefly, a gel containing AgI was covered with a diffusive gel and a 0.45 μm cellulose nitrate filter, mounted on a plastic assembly (DGT Research), and inserted into a sediment core and incubated for approximately 24 h in the temperature controlled laboratory. Sulfide in the pore water diffusing into the gel reacts with AgI to form Ag_2S, which results in a color change from yellow to black. Following incubation, the color was recorded using a conventional flat bed scanner. The sulfide concentration in the gel was determined using the calibration of Naylor et al. (2004). The pore water concentration was then derived from the estimated diffusive flux through the gel following the established procedure (e.g. Zhang et al., 1995; Naylor et al., 2004).

Additional pore water profiles were obtained using constrained Diffusive Equilibration in Thin Films (DET; Davison et al., 2000). Each probe consisted of a plastic plate containing 75 sequential isolated compartments that were 1.8 cm wide, 0.1 cm deep, and 0.1 cm across. These compartments were filled with a 1.5% agarose gel and covered with a 0.45 μm cellulose nitrate filter, creating a small scale peeper device. The probes were inserted into sediment cores and incubated for 24 h in the temperature controlled shipboard laboratory. Following incubation, the agarose gel was removed from each individual compartment and eluted in 1 ml 1 M HNO_3. The elutents were analyzed by ICP-MS. However, the small sample volumes proved too small to obtain reproducible trace metal pore water profiles, except for manganese.

3.3. Solid phase analyses

Sediment water content and density were determined from the weight loss upon freeze drying, allowing for the determination of sediment porosity. Grain size analysis was conducted using a laser diffraction technique (Malvern Mastersizer S) on freeze dried sediment following a HCl and H_2O_2 pre-treatment. Total carbon, total sulfur, and organic carbon (C_{org}; following carbonate removal with 1 M HCl) were determined on freeze-dried sediment using an elemental analyzer (LECO SC-1440H).

A total digestion with $HF–HClO_4–HNO_3$ was conducted on freeze dried sediment samples as described in Hyacinthe and Van Cappellen (2004). Determination of major elements (Ca and Al) in the extractant was

performed with inductively coupled plasma optical emission spectroscopy (ICP-OES; Perkin-Elmer Optima 3000). Analysis of metals in all extractants was carried out with ICP-MS unless otherwise noted. Acid Volatile Sulfide-Simultaneously Extractible Metal (AVS-SEM) extractions were conducted to determine concentrations of non-pyritic reduced sulfur, and metals bound to non-pyritic sulfides and other extractible phases (carbonates and amorphous oxides). AVS-SEM was performed on approximately 1 g wet sediment in an Ar-purged analysis train with room-temperature 6 M HCl for 1 h. The released H_2S was trapped in a 1 M NaOH solution from which sulfide concentrations were determined colorimetrically (Cline, 1969). It is important to note that AVS includes a range of sulfide containing compounds (Rickard and Morse, 2005). For simplicity, however, AVS is represented as iron monosulfide, FeS, in the model reaction network.

The sequential extraction method of Huerta-Diaz and Morse (1990) was performed on freeze dried samples. The method includes three operationally defined Fe and trace metal pools: reactive (1 M HCl, 16 h); silicate (10 M HF,16 h); and pyrite (conc. HNO_3, 2 h). The degree of pyritization (DOP) and degree of trace metal pyritization (DTMP) can then be calculated as follows (Boesen and Postma, 1988):

$$\mathrm{DOP}(\%) = \left(\frac{(\mathrm{pyrite}-\mathrm{Fe})}{(\mathrm{pyrite}-\mathrm{Fe})+(\mathrm{reactive}-\mathrm{Fe})}\right)\times 100 \quad (1)$$

$$\mathrm{DTMP}(\%) = \left(\frac{(\mathrm{pyrite}-\mathrm{Me})}{(\mathrm{pyrite}-\mathrm{Me})+(\mathrm{reactive}-\mathrm{Me})}\right)\times 100 \quad (2)$$

where the concentrations of Fe or trace metal (Me) measured in the reactive and pyrite pools of the extraction are used. DOP represents the percent of reactive Fe that is present as pyrite and DTMP is the percent of reactive trace metal bound in the pyrite phase. The degree of sulfidization (DOS), that is, the percent of reactive Fe that is bound to sulfide, is calculated as follows:

$$\mathrm{DOS}(\%) = \left(\frac{(\mathrm{pyrite}-\mathrm{Fe})+(\mathrm{AVS}-\mathrm{Fe})}{(\mathrm{pyrite}-\mathrm{Fe})+(\mathrm{reactive}-\mathrm{Fe})}\right)\times 100 \quad (3)$$

where (AVS–Fe) is the concentration of AVS, and reactive–Fe and pyrite–Fe are the Fe concentrations in the respective pools.

Additional extractions with citrate–dithionite bicarbonate (CDB, extraction solution analysis by ICP-OES; Slomp et al., 1996) and pH 7.5 ascorbate (Hyacinthe and Van Cappellen, 2004; Kostka and Luther, 1994) were performed on wet sediment to further characterize the reactive Fe(III) pool. The CDB extractant extracts all Fe-oxides while the near-neutral ascorbate extraction is limited to poorly crystalline and amorphous reducible Fe (III) phases. The reactive pool extraction in the Huerta-Diaz and Morse (1990) method (1 M HCl) is less specific, as it also mobilizes reactive Fe(II) phases (Kostka and Luther, 1994). The dissolution kinetics in pH 7.5 ascorbate of a freeze-dried surface sediment sample (0–0.5 cm late-summer) were followed by periodically sampling the sediment suspensions over the course of a 25-hour extraction period, following the procedure of Hyacinthe and Van Cappellen (2004).

Concentrations of Zn, Ni, Pb, and Cd, and grain size determinations for suspended matter (SPM), determined during monthly water quality monitoring performed by the Netherlands Institute for Inland Water Management and Waste Water Treatment (RIZA), were obtained from the publicly available database, www.waterbase.nl, and are reproduced here with permission. Metal concentrations in SPM reported in the data base were measured by ICP-OES after a HCl–HNO_3 extraction on freeze-dried samples. The RIZA provided SPM samples collected in 2001, on which we measured the concentrations of Fe and Mn, as these elements are not reported in the database.

3.4. Modeling

Reaction-transport model calculations were carried out with the Biogeochemical Reaction Network Simulator (BRNS; Aguilera et al., 2005; Jourabchi et al., 2005). The development and calibration of the model used to describe the sediment in Haringvliet Lake is presented in Canavan et al. (2006). The existing model, which includes a reaction network of 24 chemical species and 32 reactions, was expanded to include trace metal reactions. The discussion of reaction and transport processes in this paper is limited to those that directly involve the trace metals. Changes to model boundary conditions and rate constants for Fe, Mn, and S reactions were made to account for CDB fractions and the depositional input of a pyrite pool that were not included in the original model (Canavan et al., 2006). These changes are listed in Appendix A. Trace metals in the model were subjected to the same transport processes as other constituents, namely molecular diffusion, bioirrigation, bioturbation, and burial for solutes, and bioturbation and burial for solids. The model describes 1-D sediment profiles at steady-state. This steady-state approach was necessary as insufficient information was available to constrain time-resolved variations

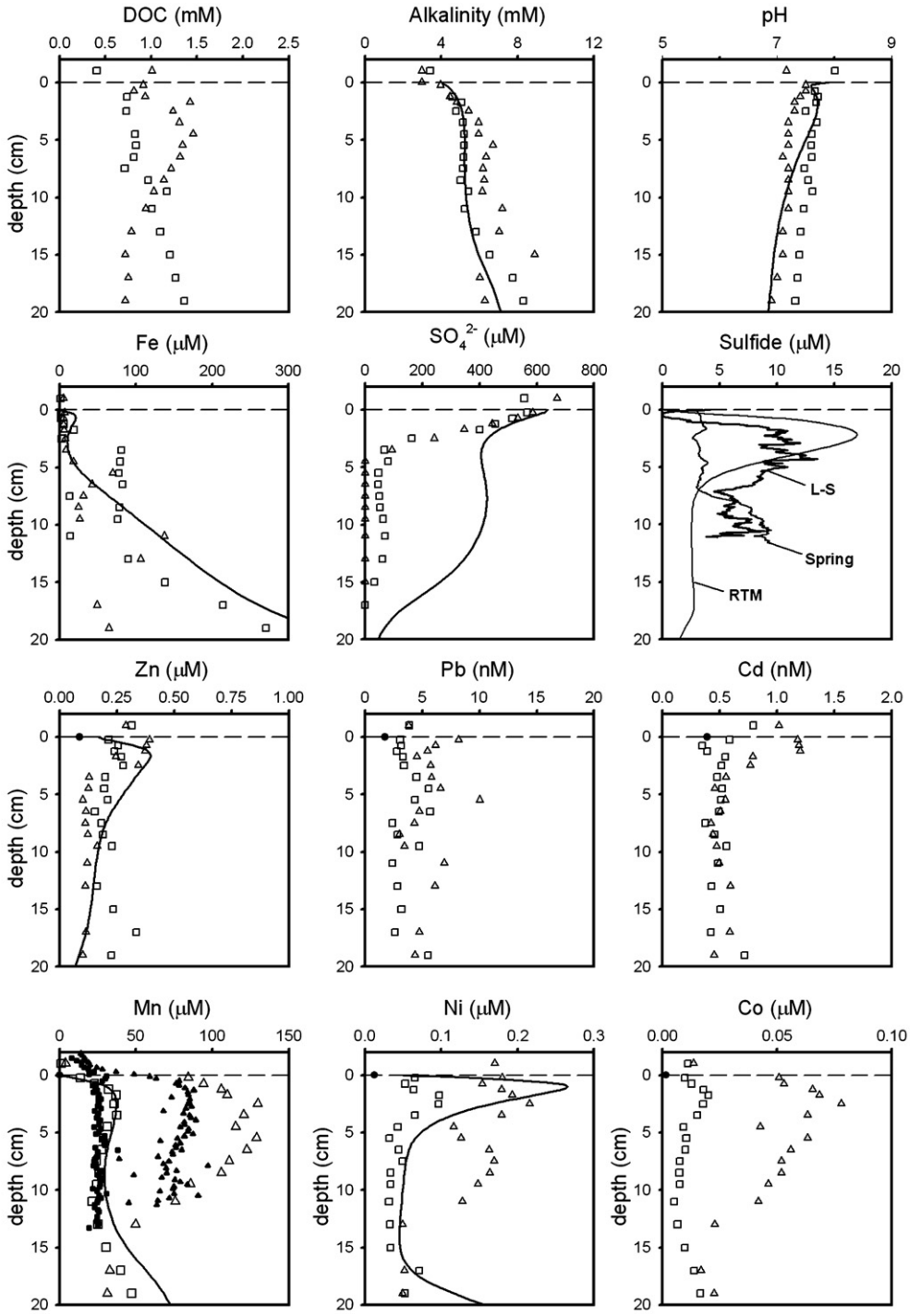

Fig. 2. Porewater profiles of DOC, alkalinity, pH, Fe, SO_4^{2-}, sulfide, Zn, Pb, Cd, Mn Ni, and Co for the late-summer (□) and spring (△) sampling times. The sediment water interface (SWI) is indicated as a broken horizontal line. Mean values of field blanks for Zn, Pb, Cd, Mn, Co, and Ni are given at the SWI (●). Model fits for alkalinity, pH, Fe^{2+}, SO_4^{2-}, sulfide, Zn^{2+}, Mn^{2+}, and Ni^{2+} are plotted as continuous lines in the plots. Pore water sulfide profiles measured with the AgI DGT probe (see Section 3.2), are also shown as continuous lines. The sulfide results from late-summer, spring, and the model are labeled L-S, spring, and RTM respectively. For Mn, the concentrations measured with constrained DET (see Section 3.2) are presented for the late-summer (■) and spring (▲).

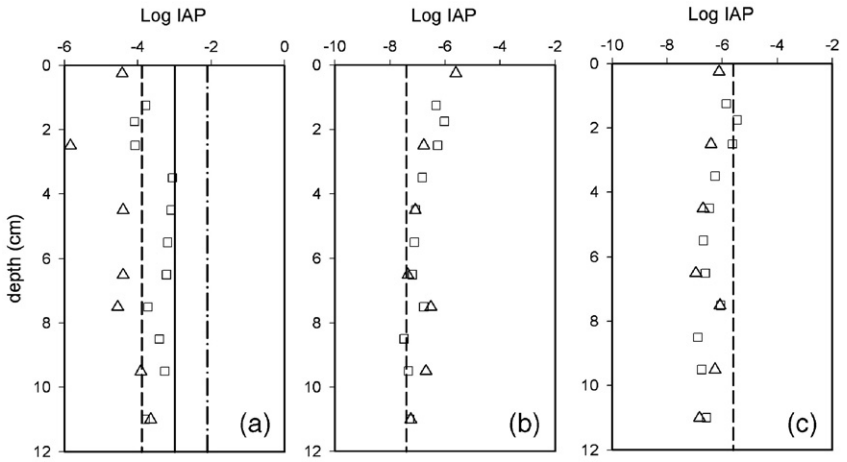

Fig. 3. Pore water ion activity products (IAP) with respect to end-member metal monosulfides for Fe (a), Co (b), and Ni (c). IAP is defined as $\{Me^{2+}\}\{HS^-\}/\{H^+\}$ and values are calculated using visual MINTEQ with pore water data from late-summer (□) and spring (△). Vertical lines represent corresponding metal sulfide solubilities (Log K_{so}) for the reaction $MeS(s)+H^+=Me^{2+}+HS^-$. Values for FeS (s) determined by Davison et al. (1999; −3.0, solid line), Benning et al. (2000; −3.9, dotted line), and Wolthers (Wolthers et al., 2005; −2.1, dash-dot line). The Log K_{so} values for CoS (s) and NiS (s) are obtained from Dyrssen and Kremling (1990; CoS = −7.4; NiS = −5.6). Solutions are super-saturated when the Log IAP value is greater than the Log K_{so}.

in bottom water chemistry and solid-phase deposition fluxes (see Canavan et al., 2006 for further discussion).

Thermodynamic speciation calculations were conducted using Visual MINTEQ (Version 2.4, this program is an adaptation of MINTEQA2; Allison et al., 1991). Calculations included the following constituents: Na^+, Ca^{2+}, Mg^{2+}, K^+, NH_4^+, SO_4^{2-}, Cl^-, PO_4^{3-}, HS^-, Alkalinity, pH, Fe^{2+}, Mn^{2+}, Co^{2+}, Ni^{2+}, Zn^{2+}, Cd^{2+}, Pb^{2+}. The ability of thermodynamic modeling to predict the speciation of dissolved metals is limited by the use of pure, end-member solid phases and, the limited knowledge of metal–sulfide stability constants. Metal complexation by dissolved organic ligands were not included in the equilibrium calculations, which may lead to overestimation of the free metal aqueous concentrations.

4. Results

4.1. Porewater

Pore water DOC displayed a gradual increase with depth in late-summer, while a subsurface maximum was observed in spring (Fig. 2). Alkalinity increased with depth in the upper 3 cm of sediment, and again below 10 cm. Pore water pH showed a gradual acidification with depth. Dissolved Fe in the pore water increased below 3 cm, with late-summer concentrations rising to 300 μM at depth. Sulfate concentrations rapidly declined in the upper 3 cm during both sampling periods. Pore water analyses based on the DGT method indicated the presences of free sulfide in the upper 10 cm of sediment. The highest sulfide concentrations (~10 μM) were observed in late-summer in the depth range 2.5–5 cm, spring sulfide concentrations increased below 7 cm. Sulfide concentrations measured colorimeterically on pore water extracted by centrifugation were below detection, probably reflecting sampling artifacts.

The pore water concentrations of Zn, Pb, and Cd were similar for the two sampling times. Both Zn and Cd

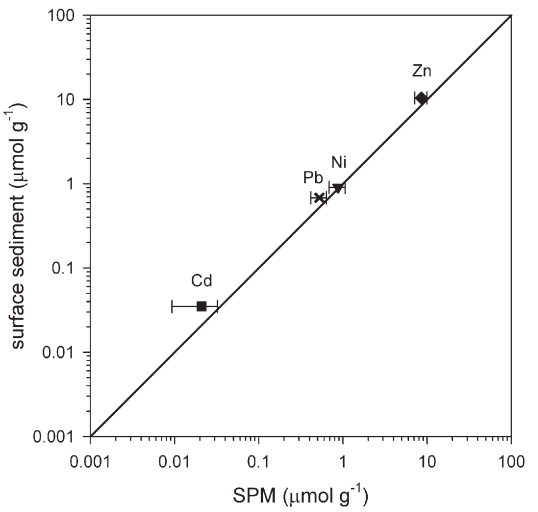

Fig. 4. The mean concentrations of Zn (◆), Pb (×), Ni (▼), and Cd (■) in suspended particulate matter (SPM) from monthly measurements between 2000–2004 (source: Rijkswaterstaat, www.waterbase.nl) versus total concentrations in the upper 2 cm of sediment (average of 3 samples). The error bars represent one standard deviation of the SPM values. A solid line represents the 1:1 relation; note the log scales.

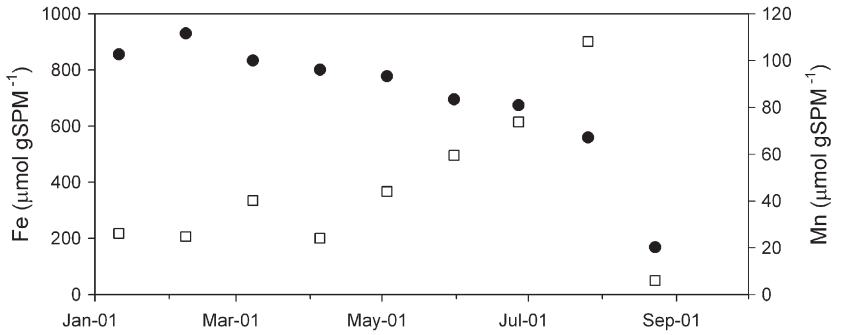

Fig. 5. Concentrations of Fe (●) and Mn (□) in suspended particulate matter (SPM) over an 8-month period in 2001.

displayed somewhat higher concentrations in the upper 3 cm. Note that the lowest pore water concentrations of Zn, Pb, and Cd approach the corresponding mean blank values, which represent practical detection limits. The pore water profiles of Mn, Ni, and Co showed subsurface maxima that were most pronounced in spring. Pore water profiles of Co and Ni resembled those of Mn, for both sampling periods. The correlation with Mn was stronger for Co ($r^2=0.92$) than for Ni ($r^2=0.81$).

The large difference in the pore water profiles of Mn, Ni, and Co between the two sampling times are unlikely to be due to the differences in the filter pore size in late-summer (0.2 μm) and spring (0.45 μm). A comparable difference in Mn pore water concentrations between the two sampling times was also observed with the constrained DET samplers which were covered with a filter membrane with a 0.45 μm pore size during both sampling times. The constrained DET profiles were in relatively good agreement with those obtained from centrifuged sediment sampling, considering that the two different techniques were performed on cores from separate box cores.

The pore waters were near equilibrium with amorphous FeS in late-summer, in the depth range 1.25–11 cm, and undersaturated in the upper 6.5 cm during spring (Fig. 3a). Supersaturation with respect to the monosulfides of Zn, Pb, and Cd was observed for both late-summer and spring, with calculated saturation indexes exceeding 2.5 (results not shown). The thermodynamic calculations predicted supersaturation to near-saturation with respect to CoS, but undersaturation with respect to NiS (Fig. 3b–c). The pore waters remained highly undersaturated with respect to MnS (saturation index <- 3).

4.2. SPM metal content

Trace metals in the water column of the Haringvliet Lake are mainly associated with the SPM. Concentrations of solid-phase Zn, Ni, Pb, and Cd in the upper 2 cm of sediment exhibit the same order of abundance and the same magnitudes as in the lake SPM (Fig. 4). Concentrations of Fe and Mn in the SPM varied independently from one another (Fig. 5), as previously observed at other sites in the Rhine–Meuse Delta (Paalman and van der Weijden, 1992). Both Fe and Mn SPM concentrations declined sharply in August 2001, as a result of dilution by an algal bloom in the lake.

The SPM trace metal concentrations varied substantially in the period 2000–2004, with coefficients of variation ranging from 17% for Zn to 55% for Cd (see error bars on Fig. 4). The concentrations of Zn and Pb followed similar trends during this period ($r^2=0.84$), while

Table 1
Depth weighted average concentrations of organic carbon (C_{org}), Ca, Al, Fe, porosity and grain size in the upper 10 cm of sediment and correlations with grain size

C_{org}	Ca	Al	Fe	Porosity	Grain size <63 μm
% dry weight				(vol.%)	% total
4.1 (0.11)	3.6 (0.10)	4.1 (0.05)	1.9 (0.03)	84 (2.15)	93 (2.00)
r^2 for regression with grain size less than 65 μm (%)					
0.62*	0.01	0.58*	0.89*	0.75*	–

Al and Fe were determined on 11 samples, the remaining values were determined on 12 samples. Values in parentheses are one standard deviation. Correlation determined with data from the upper 30 cm of sediment (19 samples).
*Denotes significant correlation ($P<0.05$).

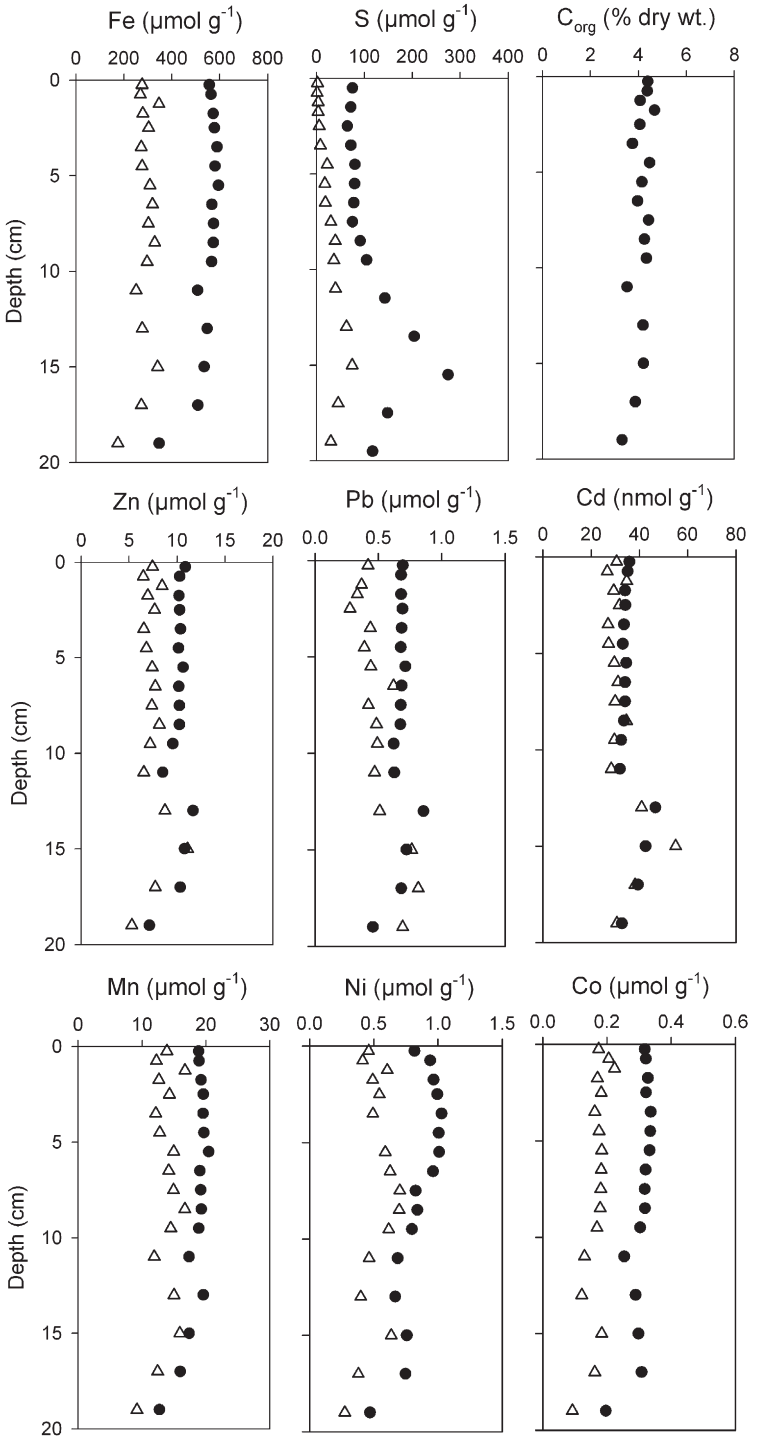

Fig. 6. Depth distributions of sediment concentrations of Fe, S, C_{org}, Zn, Pb, Cd, Mn, Ni, and, Co, in late-summer. Total concentrations (●) and concentrations from the acid volatile sulfide-simultaneously extractable metals (AVS-SEM; 6 M HCl) (△) are shown.

correlations between Zn and Ni ($r^2 = 0.43$), and Zn and Cd ($r^2 = 0.37$) were substantially weaker. The trace metal SPM concentrations displayed negative correlations with SPM organic matter content; indicating that organic matter produced in the lake during algae blooms had a lower trace metal content than the terrestrially derived SPM.

4.3. Sediment solid phase

The sediment is highly porous, fined grained and organic rich (Table 1). Porosity and sediment concentrations of total Al, Fe, and C_{org} were correlated with grain-size, while the total Ca concentration did not (Table 1). The total sediment profiles of C_{org}, Fe, Mn, Zn, Pb, Co, and Cd displayed little variation with depth, particularly in the upper 10 cm of sediment (Fig. 6). The total Ni concentration showed a slight depletion in the uppermost cm of sediment.

As expected, the AVS-SEM concentrations were lower than the respective total concentrations (Fig. 6). The SEM concentrations were nearly equal to the total concentrations for Cd, while the refractory pools not extracted by 6 M HCl were most significant for Fe, Ni, and Co. The differences between the SEM and total concentrations declined with depth, except for Fe, S, and Co. The total sulfur concentration increased sharply below 10 cm to a peak concentration at a depth of approximately 15 cm. The concentration of AVS was near zero in the upper 2 cm of sediment and, like total *S*, increased with depth until 15 cm depth. Pore water sulfide accounted for no more than 1% of AVS based on the DGT sulfide profiles.

The concentrations released by the reductive extractions (ascorbate, CDB) declined with depth for all metals (Fig. 7). Significantly higher concentrations of Fe, Mn, Ni, and Co were extracted in CDB than in near-neutral ascorbate. For Zn, the two extractions yielded similar concentrations, which accounted for 15% of the total zinc at the sediment surface. The concentrations of CDB extractable Fe, Ni, and Co declined more sharply with depth than the ascorbate extractable concentrations. Both extractions suggested the persistence of reducible compounds at 20 cm depth. At the sediment surface (0–0.5 cm) the CDB fraction accounted for 68% of total Mn, 42% of total Fe, 34% of total Co and 23% of total Ni. Reducible phases appeared to be less important for Pb and Cd, as ascorbate extractions released only 7% and 0.3% of the total surface sediment concentration, respectively (Pb and Cd concentrations were not determined in the CDB extractions).

The release of trace metals during the kinetic extraction with pH 7.5 ascorbate performed on the topmost

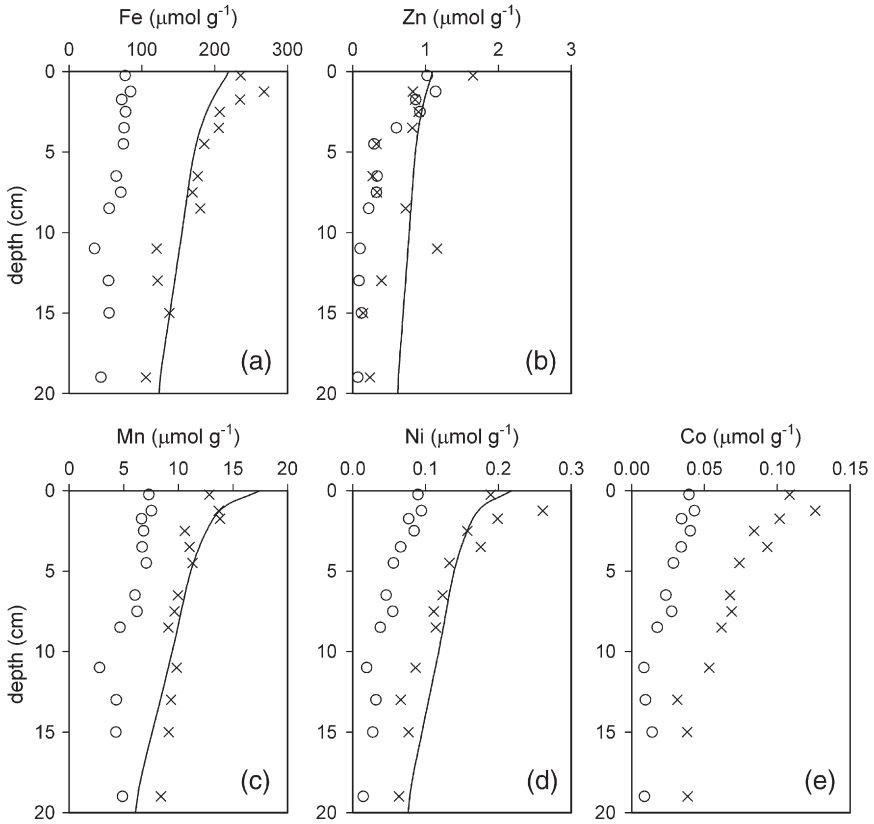

Fig. 7. Sediment distributions of ascorbate (○) and CDB (×) extractable Fe (a), Zn (b), Mn (c), Ni (d), and Co (e) from sediment collected in late-summer. Model distributions of $\Sigma Fe(OH)_3$ (a), $Fe(OH)_3$–Zn (b), ΣMnO_2 (c), and MnO_2–Ni (d) are given as solid lines in the respective plots.

(0–0.5 cm) sediment displayed a number of distinct patterns. These are shown in Fig. 8 where the extracted concentrations of dissolved trace metal are plotted versus the extracted concentration of dissolved Fe. The latter increased continuously over the 25 h of extraction. The concentrations of extracted Zn, Co and Mn correlated

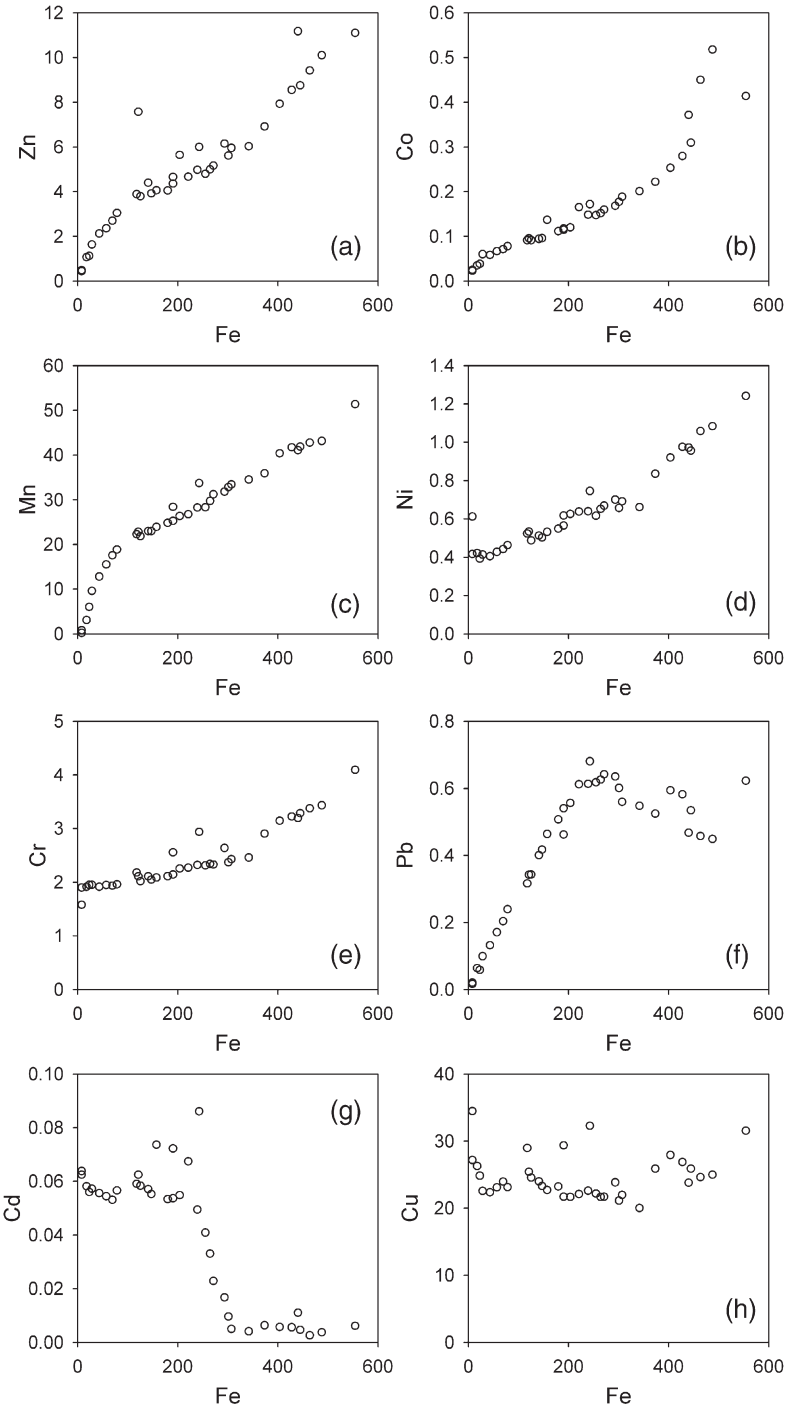

Fig. 8. Extraction solution concentrations of Zn (a), Co (b), Mn (c), Ni (d), Cr (e), Pb (f), Cd (g), Cu (h) versus that of Fe in the kinetic ascorbate extraction. All concentrations are given in μmol l^{-1}. Samples were collected periodically over a 25-hour extraction conducted on a freeze-dried sediment sample from 0–0.5 cm depth collected in late-summer.

Table 2
Calculated degree of pyritization (DOP), Degree of Sulfidization (DOS), and degree of trace metal pyritization (DTMP)[a] from sediment collected in late-summer

Depth range			DTMP				
	DOP	DOS	Mn	Zn	Pb	Ni	Co
(cm)				(%)			
0–1	13.7	14.9	1.1	6.8	9.3	13.3	7.7
1–2	11.9	14.4	0.9	5.6	9.4	10.2	7.0
2–3	12.8	16.2	0.8	6.1	2.7		8.1
3–4	13.8	18.9	1.0	6.0	8.5	11.6	9.0
5–6	15.7	26.6	1.0	5.4	7.7	12.8	9.8
7–8	14.0	31.9	0.9	6.2	6.0	10.9	10.6
9–10	22.5	42.7	1.4	5.2	7.2	13.0	14.4
12–14	35.2	59.8	2.6	5.8	6.3	21.2	26.6
16–18	15.1	50.6	1.1	6.1	4.8	15.6	16.2

DOP is calculated using the 1 M HCl extraction (Huerta-Diaz and Morse, 1990).
[a] DTMP values for Cd are not reported due to evidence of contamination. Values ranging from 0.4–8.0% were found at an additional sample site in the lake.

positively with that of Fe during the entire extraction. Ni and Cr showed a near-instantaneous release to solution at the start of the extraction, followed by continuous release for the remainder of the extraction. Cu and Cd release was entirely uncorrelated to that of Fe, while the trends of Pb and Cd indicated of removal by precipitation when dissolved Fe exceeded 250 μM.

The degree of pyritization (DOP) in the upper 8 cm of sediment ranged between 12 and 16% (Table 2), followed by an increase to 35% at 15 cm. The degree of sulfidization increased between 2 and 15 cm, reaching a maximum value at the same depth as AVS. The degree of trace metal pyritization (DTMP) of Mn never exceeded 3%, while those of Zn, Pb, and Cd values remained below 10%. Higher DTMP values were obtained for Ni (10–21%) and Co (7–26%). In addition, the DTMP values of Ni and Co increased with increasing DOP, while those of the other metals did not correlate with DOP.

5. Discussion

5.1. Pore water profiles

The build up of alkalinity in the pore waters reflects C_{org} mineralization (Fig. 2). The alkalinity increase with depth, however, is not monotonic because of pore water irrigation in the upper 10–15 cm (Canavan et al., 2006). Our previous work has shown that sulfate reduction is an important mineralization pathway (Canavan et al., 2006), which explains the rapid depletion of pore water SO_4^{2-} and the presence of measurable free sulfide. The pore water profiles of SO_4^{2-}, sulfide and dissolved Fe imply overlapping zones of sulfate and Fe(III) reduction. Such overlap is observed in many sedimentary environments, and is attributed to the wide range in properties of natural Fe(III) mineral assemblages (Postma and Jakobsen, 1996; Roden, 2003) and sediment mixing processes (Thullner et al., 2005).

The pore water profiles of Zn, Pb, and Cd show a near-surface enrichment in spring (Fig. 2). For Cd, release from freshly deposited OM is a possible mechanism explaining the near-surface pore water enrichment in spring. The chemical extraction results indicate that little Cd is associated with the reducible pool of Fe and Mn oxides (Fig. 6), and no correlation is observed between Cd and Fe release during the ascorbate extractions (Fig. 8). These findings agree with the reported association of Cd with organic matter in estuarine sediments (Audry et al., 2006). For Zn and Pb, the reductive extraction results imply that the near-surface pore water enrichments can, in part, be explained by reductive dissolution of reactive Fe and Mn oxide phases close to the sediment–water interface. The concentrations of Zn and Pb in SPM of Haringvliet Lake are also strongly correlated ($r^2 = 0.84$), suggesting similar associations of the two metals in particulate matter settling to the lake bottom.

The increased concentrations of Mn, Ni, and Co in spring could be due to variations in Mn-oxide deposition. As shown in Fig. 5, large fluctuations in the Mn content of SPM are observed in Haringvliet Lake. The linear correlations between the pore water concentrations of Co and Ni with those of Mn, suggest that the release of the trace metals are coupled to Mn reduction. However, the concentration ratios of Mn to Co and Ni in the pore waters (approximately 2000 and 700, respectively) are much higher than those measured in the reductive

extractions (Mn:Co = 100–450 and Mn:Ni = 50–155). We attribute this to the more efficient removal of dissolved Co and Ni by sulfide precipitation (Fig. 3, Table 2), compared to Mn (see next section).

5.2. Sediment solid phase

The correlations of sediment C_{org}, Al, and Fe concentrations with grain size <63 μm (Table 1) indicate a close association of OM, metal oxides and clay minerals (Tessier et al., 1996). The surface sediment concentrations at the study site exceed the Dutch sediment quality target values by a factor of 6 for Co, and 3 for Zn and Ni. The concentration of Cd is approximately 1.6 times the target value, while Pb concentrations are just below the quality goal concentration of 0.7 μmol g^{-1}. The concentrations of target values for of the Dutch Soil Protection Act are calibrated to the clay and organic matter contents at the sample site.

Although pore water profiles suggest diagenetic remobilization may occur in the sediment (Fig. 2), those processes to not result in a redistribution of the total sediment concentration profiles, with the exceptions of S and possibly Ni (Fig. 6). Total sediment Ni concentrations are greater in the depth range 2–6 cm than in the sediment directly above and below this zone. This may reflect either a changing total Ni input to the sediment over time, or post-depositional redistribution. Total S and AVS display a peak concentration at 15 cm, which is likely the result of sulfate reduction with subsequent precipitation of metal sulfides, primarily FeS and FeS_2. However, steady-state model simulations are unable to reproduce the observed AVS peak, indicating that historical variations in depositional conditions have also affected the sediment depth profiles (Canavan et al., 2006).

The decreasing concentrations with increasing depth of the ascorbate and CDB extractable Fe pools are consistent with reductive dissolution of Fe(III) in the sediment (Fig. 7). The reduction of chemically reducible Fe (III) mineral phases is not complete by 20 cm depth, however indicating slow dissolution kinetics despite the reducing conditions. Similar results have been reported for other freshwater sediments (Hyacinthe and Van Cappellen, 2004). The progressive decrease with depth of the ascorbate and CDB extractable concentrations of Mn, Zn, Ni, and Co also indicate release from reducible mineral phases (Fig. 7). This is consistent with the positive correlations of the concentrations of these metals with that of Fe released during the kinetic ascorbate extraction from surface sediment.

SPM concentrations of Fe and Mn in the water column are decoupled (Fig. 5). The increasing trend from winter to summer of the Mn SPM concentration in 2001 (Fig. 5) can be explained by increased release of Mn^{2+} from the more reducing sediments in summer and faster Mn^{2+} oxidation in the warmer water column (Paalman and van der Weijden, 1992). However, in the sediment, reducible Mn and Fe concentrations appear to be coupled to one another (Figs. 7 and 8), probably because of co-precipitation during Fe and Mn oxidation in the uppermost sediment. Much of the reducible Mn is found in the ascorbate pool (Fig. 7), which includes both oxide phases formed in the water column and in the sediment.

While the pore water profiles indicate a close coupling of Ni and Co to Mn (Fig. 2), the kinetic ascorbate extraction reveals a different nature of the association of the trace metals with Mn (Fig. 8). In particular, Ni shows a significant initial release to solution that is not accompanied by similar releases of Mn and Co, suggesting the presence of a significant loosely sorbed fraction of Ni. These observations are consistent with the results of Kay et al. (2001), who report that Co uptake by Mn oxides is due to incorporation in the crystal structure, while Ni is removed through adsorption at the mineral surface.

In contrast to the other metals shown in Fig. 7, Zn concentrations are similar in the CDB and ascorbate extractions. Thus, Zn is incorporated into newly forming poorly crystalline, precipitating mineral phases in the surface sediment, but is not present in the more crystalline oxides extracted by CDB. Pb and Cd concentrations recovered in the ascorbate extraction are low relative to their total concentration (7% and 0.3%, respectively, in the 0–0.5 cm depth interval). As noted before, the release of Cd is not related to the reductive dissolution of Fe (Fig. 8).

The DOP values of 12–14% near the sediment surface suggest that part of the pyrite in the sediment may be from detrital deposition or sediment resuspension in addition to formation in the sediment (Table 2). Values of DOP and DOS show that much of the iron in the sediment is not associated with sulfide, which is consistent with the relatively high concentrations of reducible Fe measured over the entire depth range investigated (Fig. 7). Our DTMP results are similar to those reported by Morse and Luther (1999), who attribute the commonly found low DTMP values for Zn, Pb, Cd to the tendency of these metals to form monosulfide phases. The higher DTMP values for Ni and Co reflect their partial incorporation into pyrite. Additionally, FeS may also bind Ni and Co (Huerta-Diaz et al., 1998; Morse and Arakaki, 1993), while Zn, Pb, and Cd may substitute for Fe resulting in trace metal monosulfides (Di Toro et al., 1990). The low DTMP values found for Mn (Table 2) are characteristic for sediments with DOP values less than 35% (Morse and Luther, 1999).

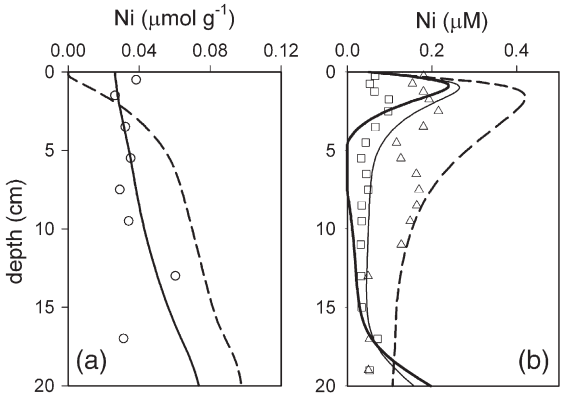

Fig. 9. (a) Depth distribution of Ni from the pyrite fraction of the Huerta-Diaz and Morse (1990) extraction (○). The solid line represent the modeled concentration of pyrite-associated Ni. The dashed line is the modeled concentration of FeS associated Ni, which is not constrained by extraction data. (b) Pore water concentrations of Ni from late-summer (□) and spring (△). Modeled concentration of Ni^{2+} with FeS–Ni ratio (see text) set to 588 (heavy line), 833 (thin line), and 1100 (dashed line).

5.3. Diagenetic modeling

Reactive transport model calculations are used to simulate the changes in speciation of Zn and Ni with depth, to explore the sensitivity of burial and sediment–water exchange fluxes of the metals, and predict their response to environmental changes that are expected to accompany estuarine restoration in the Haringvliet. Additional metals are not included for the sake of simplicity. The modeled present-day steady state concentration profiles of the pore water and reactive solid-state metals generally fall within the ranges of measured values (Figs. 2, 7 and 9). As the lake sediments obviously do not represent steady state conditions, a perfect match to the measured data is not possible.

The reaction and transport processes of Zn and Ni included in the model are described in Table 3 and parameter values are given in Table 4. For Zn, three parameters are used as fitting parameters. These are the rate constants for ZnS precipitation, Zn substitution of Fe in FeS, and ZnS oxidation with O_2. For Ni, only the molar ratio describing Ni sorption to FeS was adjusted when fitting the data.

The model derived Zn^{2+} pore water profile exhibits a sub-surface maximum and generally follows the trend observed in the data (Fig. 2). The model $Fe(OH)_3$–Zn pool size declines with depth, although the model underestimates the drop in concentration observed in the reductive extractions (Fig. 7b). ZnS concentrations

Table 3
A description of trace metal reaction–transport processes, the numbering corresponds with that given in Fig. 10

	Processes	Description
1	Deposition	Influx of metals is related to the influx of Fe-oxides (Zn), Mn-oxides (Ni), or FeS_2 (Ni) by a ratio derived from extractions
2	Reductive dissolution	Trace metal is released from oxides by reductive dissolution. The initial model includes two separate fractions of Fe and Mn-oxides. One fraction that can be reduced in conjunction with bacterial OM degradation and by reaction with sulfide. The second fraction is only reduced by sulfide. A single oxide-trace metal ratio is applied to both oxide pools
3	Oxide formation	Mn^{2+} and Fe^{2+} can oxidatively precipitate by reaction with O_2. This process was modeled to remove dissolved trace metal with the same oxide-trace metal ratio found in the incoming material
4	Bioirrigation	The flushing of burrows by benthic organisms in the sediment is modeled as a non-local exchange process: α_x ($[Me]_x - [Me]_{OLW}$) where α_x is the bioirrigation coefficient at depth x, $[Me]_x$ is the concentration of dissolved trace metal at depth x, and $[Me]_{OLW}$ is the concentration of dissolved trace metal in the overlying water
5	Diffusion	Transport by molecular diffusion of solutes is included in the model. The diffusion of trace metal is determined for the upper and lower boundaries
6	Precipitation (ZnS)	The precipitation of ZnS is included by the rate expression $k_{ZnSprecip}$ (($[Zn^{2+}][HS^-]/[H^+]K_{ZnS}) - 1$) where $k_{ZnSprecip}$ is a rate constant and K_{ZnS} is the equilibrium constant. This reaction is set to zero when ZnS is undersaturated
7	Displacement	The displacement of Fe by Zn in FeS is included by the rate expression: k_{disp} $[Zn^{2+}]$ FeS(s) where k_{disp} is a rate constant
8	Adsorption	The adsorption of Ni^{2+} to FeS and to FeS_2 is related to the rate of formation of FeS and FeS_2 by FeS:Ni and FeS_2:Ni ratios. The formation of FeS_2 is modeled as a reaction of FeS and sulfide. This process results in the release of Ni from FeS and subsequent removal by FeS_2, where the process results in a net removal
9	Oxidative dissolution	ZnS oxidation with O_2 is included by the rate expression: k_{ZnSox} $[O_2]$ ZnS(s) where k_{ZnSox} is a rate constant. The release of Ni^{2+} is related to the dissolution and oxidation of FeS by the FeS:Ni ratio. Note that the oxidation of FeS_2 is not included in the model
10	Burial	Burial of solids is determined at the lower boundary (20 cm)

Model parameters for trace metals are further defined in Table 4.

Table 4
Description and values of model parameters that relate to processes affecting trace metals and the depth distributions of the bioirrigation coefficient, α. and bioturbation coefficient, D_b

Parameter	Value	Units	Description
x	0–20	cm	Depth in cm
α_0	10	yr^{-1}	The bioirrigation coefficient at the sediment surface. The value of α is depth dependant (see below)
D_{b0}	5	$cm^2\ yr^{-1}$	Bioturbation coefficient at sediment surface
λ	2.5	cm^{-1}	D_b depth attenuation coefficient
Fe:Zn	200	$mol\ mol^{-1}$	Ratio of Fe:Zn in Fe-oxides, based on extraction results and used in processes 1–3 (Fig. 10, Table 3)
Mn:Ni	80	$mol\ mol^{-1}$	Ratio of Mn:Ni in Mn-oxides, based on extraction results and used in processes 1–3 (Fig. 10, Table 3)
$k_{Znprecip}$	1.0×10^{-10}	$mol\ g^{-1}\ yr^{-1}$	Rate constant for ZnS precipitation, used as a fitting parameter
K_{ZnS}	$10^{-9.02}$		The equilibrium constant for ZnS as reported in (Huerta-Diaz et al., 1998)
k_{disp}	1.0×10^{3}	yr^{-1}	Rate constant for Zn displacement of Fe in FeS, used as a fitting parameter
k_{ZnSox}	1.0×10^{5}	$mol^{-1}\ L\ yr^{-1}$	Rate constant for ZnS oxidation with O_2, used as a fitting parameter
FeS:Ni	833	$mol\ mol^{-1}$	Molar ratio of Ni adsorption to FeS, used as a fitting parameter
FeS_2:Ni	600	$mol\ mol^{-1}$	Ratio of Fe:Ni found in the HNO_3 extraction step of the Huerta-Diaz and Morse (1990) extraction

Depth distribution of α, D_b	Description
$\alpha = \begin{cases} \alpha_0\left(1-e^{(x-17)}\right) & (x\leq 17\text{cm}) \\ 0 (x>17\text{cm}) \end{cases}$	Depth distribution of the bioirrigation coefficient α.
$D_b = D_{b0}e^{-(x/\lambda)}$	Distribution of bioturbation coefficient D_b

increase from 0.04 to 0.5 μmol g dry wt.$^{-1}$, in parallel to the decrease of the Fe-oxide bound pool. Since the pore waters are super-saturated with respect to ZnS, very low values of the rate constant for ZnS precipitation are required to maintain Zn^{2+} concentrations in the observed range (Table 4). Processes that slow or inhibit the reaction between dissolved Zn and sulfide, such as Zn^{2+} binding to DOC, are implicitly included in this rate constant.

ZnS oxidation and Zn^{2+} scavenging by newly formed oxides in the sediment are important processes occurring in the upper millimeters of sediment, due to the shallow O_2 penetration depth (~4–7 mm; Canavan et al., 2006). The diffusive flux of Zn^{2+} from the sediment to the overlying water (OLW) is sensitive to the rates of these processes. ZnS oxidation contributes significantly to the release of Zn^{2+} in the upper millimeters of sediment and, consequently, strongly modulates Zn^{2+} fluxes at the SWI. In a simulation run without ZnS oxidation the flux of dissolved Zn^{2+} across the SWI changed from an efflux of 24 nmol $cm^{-2}\ yr^{-1}$ to an influx of 9 nmol $cm^{-2}\ yr^{-1}$ into the sediment. Model results predict that 40% of the deposited Fe-oxide bound Zn is converted to ZnS (Fig. 10a).

The modeled Ni^{2+} pore water concentrations are in the range measured in the upper 16 cm of the sediment, although the modeled peak concentration is greater than observed and the peak occurs over a more narrow depth range (Fig. 2). Modeled concentrations of Ni^{2+} are greater than measured values below 16 cm. Model concentrations of Ni associated with Mn-oxides are in reasonable agreement with CDB-extractable Ni concentrations (Fig. 7d). The model derived FeS_2:Ni concentrations are similar to the extraction results in the upper 10 cm

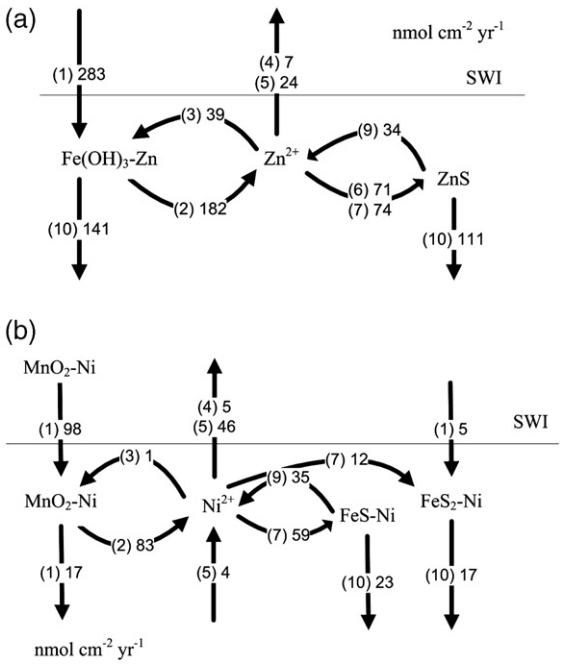

Fig. 10. Schematic representations of the model reaction and transport processes for Zn (a) and Ni (b). The bracketed numbers refer to the description of processes given in Table 3. Process rates are integrated over the upper 20 cm of sediment. Rates and fluxes are given on the arrows in units of nmol $cm^{-2}\ yr^{-1}$; discrepancies in mass balance are a result of rounding.

(Fig. 9a). The peak in FeS_2 (Table 2, DOP) and associated Ni below 10 cm cannot be reproduced by the steady-state model, however. The ratio of FeS:Ni is estimated at 833 through model fitting of the pore water Ni^{2+} profile. This ratio is at the low end of the range of values found in sulfidic precipitates on Teflon sheets incubated in fresh water lakes in Canada ($1.0\times10^3-2.0\times10^6$; Huerta-Diaz et al., 1993; Huerta-Diaz et al., 1998). The modeled pore water Ni^{2+} concentration profile is quite sensitive to changes in the FeS:Ni ratio (Fig. 9b). Decreasing the ratio value results in complete removal of Ni from the pore water and alters the mass balance of Ni in the model. A FeS:Ni ratio of 1100 results in Ni^{2+} concentrations that are greater than the measured values.

Model results suggest that only 17% of the deposited Mn-oxide bound Ni is buried in that form (Fig. 10b). Of the Ni released from Mn-oxides, 37% binds to FeS or FeS_2. An additional 30% of the FeS_2:Ni pool is derived from deposition. Pore water Ni^{2+} that is not removed through precipitation with sulfides mostly escapes from the sediment through diffusion or bioirrigation. The Ni^{2+} efflux from the sediment is estimated to be approximately 50% of the deposition flux of reactive Ni from the water column.

The simple steady-state model calculations in this study represent an initial step in the process of describing the complex and dynamic trace metal cycling in the sediments. However, even at this stage, the model results for Zn and Ni provide valuable information. While sediment efflux of Ni^{2+} corresponds to 50% of the reactive Ni input flux, it is only 11% in the case of Zn, implying a higher retention efficiency of Zn in the sediment (Fig. 10). It is important to remember that modeled trace metal input fluxes represent only the fraction associated with reactive Fe and Mn-oxides. Thus the total metal input fluxes are higher than the reactive metal input fluxes. The increased mobility of Ni relative to Zn can be explained by differences in removal by oxide formation and oxidative dissolution of sulfides. In the model, Ni^{2+} is removed by newly formed Mn-oxides, which precipitate at a slower rate than Fe-oxides. Therefore, the *in-situ* Zn and Ni behavior may not differ as greatly as suggested by the model calculations, because Zn^{2+} and Ni^{2+} can be scavenged by Fe and Mn-oxides. The sediment extractions further suggest a mixed Fe/Mn-oxide phase forming in the surface sediment.

The oxidation and dissolution of FeS occurs more readily than that of ZnS, allowing for a greater release of Ni associated with FeS than precipitated ZnS. Metal release via sulfide oxidation occurs primarily in the upper millimeters of sediment, which allows for diffusion across the SWI. Bioirrigation is responsible for less transport of metal to the OLW than diffusion for both Zn and Ni. The low rate of transport via bioirrigation is due to the similarity in concentration of bottom water and average pore water.

Additional simulations assess the sensitivity of the model to increased sulfate availability and bioturbation (Table 5). These changes are expected to accompany estuarine restoration as marine waters contain higher sulfate concentrations and higher bottom water salinity is expected to change the composition of the benthic community at the site, resulting in increased bioturbation. Increased sulfate concentrations in the OLW favor sulfate reduction in the sediment, elevating sulfide concentrations. Increasing sediment mixing also results in increased sulfate reduction as reactive OM is mixed below the depth of oxygen penetration. In these scenarios, the formation of ZnS and Ni adsorption to Fe-sulfides increases up to 35% and 26%, respectively, in response to the increased sulfide production in the sediment. Increased mixing at the sediment surface ($+D_{b0}$) leads to a greater rate of FeS oxidation allowing for a slight increase in Ni efflux, despite a greater adsorption of Ni to Fe-sulfides. This is not observed for Zn because ZnS oxidation occurs more slowly than FeS. The simulated changes to sediment processes resulting from estuarine restoration are shown to have a greater effect on the solid phase speciation than on metal efflux.

Table 5
The net rates of ZnS precipitation, Ni adsorption to Fe-sulfides, and release to the overlying water in simulations with increased sulfate availability in the overlying water, increased bioturbation intensity (D_{b0}) and deeper bioturbation (λ)

Scenario	ZnS precipitation	Zn^{2+} efflux to OLW	Ni^{2+} adsorption to FeS and FeS_2	Ni^{2+} efflux to OLW
	nmol cm^{-2} yr^{-1}			
Initial conditions[a]	110	31	62	51
$+SO_4^{2-}$ (10 mM)	122	27	63	51
$+D_{b0}$ (10 cm^2 yr^{-1})	133	31	74	54
$+\lambda$ (5 cm^{-1})	114	31	65	52
$+D_{b0}$ and $+\lambda$	137	30	78	55
$+D_{b0}$, $+\lambda$, $+SO_4^{2-}$	148	24	78	55

[a] Initial conditions: SO_4^{2-} in OLW 0.638 mM, $D_{b0}=5$ cm^2 yr^{-1}, $\lambda=2.5$ cm^{-1}.

6. Conclusions

The Haringvliet Lake sediment exhibits elevated concentrations of trace metals (Cd, Co, Ni, Pb, and Zn) derived from riverine suspended particles. Results of extractions show declining concentrations of reducible phases and an increase in sulfide species with depth. Pore waters are supersaturated with respect to Zn, Pb, Co, and Cd monosulfides, while Ni and Co are found to be associated with pyrite. These results illustrate a transition from oxide-bound to sulfide-bound trace metals with depth in the sediment. Total metal sediment profiles suggest that little metal release from the sediment is occurring with the possible exception of Ni. Diagenetic model simulations predict a greater mobility of Ni than Zn, as Ni does not form stable metal-sulfides, and is more slowly removed by oxidative precipitation at the sediment surface. Upon restoration of estuarine conditions, sulfide phases may become increasingly important for sediment trace metal speciation, while trace metal efflux should be relatively unaffected.

Acknowledgements

We gratefully acknowledge the crew of R.V. Navicula and members of the Utrecht University geochemistry research group for their help in the field and in the laboratory. We thank Erik van Vilsteren for conducting the ICP-MS measurements. The manuscript benefited from discussions with Jos Vink and commentary from André Tessier. The Netherlands Institute for Inland Water Management and Waste Water Treatment (RIZA) financially supported the field work, RWC, GvdB, and JJGZ, and granted permission for the use of data from www.waterbase.nl. The Netherlands Organization for Scientific Research (NWO) provided support through the Pioneer program to PVC. CPS was supported by a fellowship of the Royal Netherlands Academy of Arts and Sciences (KNAW).

Appendix A

The model concentrations of Fe and Mn-oxides in the original model (Canavan et al., 2006) were fit to the ascorbate extraction values because the CDB values were not available. The depositional flux of $Fe(OH)_3B$ and MnO_2B are increased in this simulation to approximate the results of the CDB extraction. (The model contains two pools of Fe and Mn-oxides: pool A can be reduced by reaction with organic matter and sulfide, pool B is only reactive with sulfide.) An input flux of FeS_2 (pyrite) is included in the model to better fit the concentrations obtained from the Huerta-Diaz and Morse (1990) extraction. Based on the conditions in the lake and river system we believe this pyrite is not formed in the water column. Possible sources of pyrite in the SPM include the wind-driven resuspension of sediment within the lake and from upstream sediments. The changes to the inputs of Fe and Mn necessitated the adjustment of other parameters to best fit the profiles of Fe^{2+}, Mn^{2+}, ΣHS^- H_2S, and FeS. The parameters are described and the new values are presented in Table A1.

Table A1
Changes in boundary conditions and parameter values from the model presented in Canavan et al. (2006)

Species	Units	Current	Previous	Description
MnO_2B	$\mu mol\ cm^{-2}\ yr^{-1}$	3.7	2.1	Depositional flux
$Fe(OH)_3B$	$\mu mol\ cm^{-2}\ yr^{-1}$	42.0	23.1	Depositional flux
FeS_2	$\mu mol\ cm^{-2}\ yr^{-1}$	3.2	0.0	Depositional flux
$KmFe(OH)_3$	$\mu mol\ g^{-1}$	500	200	Limiting concentration for Fe-reduction with OM
Kfemn	$\mu M\ yr^{-1}$	1×10^{-2}	1×10^{-1}	Rate constant for the reduction of MnO_2 by Fe^{2+}
Ktsmn	$\mu M\ yr^{-1}$	4×10^{-3}	7.5×10^{-3}	Rate constant for the reduction of MnO_2 by sulfide
Ktsfe	$\mu M\ yr^{-1}$	8×10^{-4}	2.5×10^{-3}	Rate constant for the reduction of $Fe(OH)_3$ by sulfide
Kfespre	$mol\ g^{-1}\ yr^{-1}$	7.5×10^{-4}	1.5×10^{-3}	Rate constant for the formation of FeS(s) from Fe^{2+} and sulfide
Kpyrpre	$\mu M\ yr^{-1}$	9×10^{-3}	3.3×10^{-3}	Rate constant for the formation of FeS_2(s) from FeS(s) and sulfide

References

Aguilera DR, Jourabchi P, Spiteri C, Regnier P. A knowledge-based reactive transport approach for the simulation of biogeochemical dynamics in earth systems. Geochem Geophys Geosyst 2005;6:Q07012.

Allison JD, Brown DS, Novo-Gradac KJ. MINTEQA2/PRODEFA2, a geochemical assessment model for environmental systems: Version 3.0 users manual. US EPA; 1991.

Audry S, Blanc G, Schafer J, Chaillou G, Robert S. Early diagenesis of trace metals (Cd, Cu, Co, Ni, U, Mo, and V) in the freshwater reaches of a macrotidal estuary. Geochim Cosmochim Acta 2006;70:2264.

Baird C, Cann M. Environmental chemistry. New York: W.H. Freeman and Company; 2005. 653 pp.

Benning LG, Wilkin RT, Barnes HL. Reaction pathways in the Fe–S system below 100 degrees C. Chem Geol 2000;167:25–51.

Boesen C, Postma D. Pyrite formation in anoxic environments of the Baltic. Am J Sci 1988;288:575–603.

Boudreau BP. Metals and models: diagenetic modelling in freshwater lacustrine sediments. J Paleolimnol 1999;22:227–51.

Canavan RW, Slomp CP, Jourabchi P, Van Cappellen P, Laverman AM, van den Berg GA. Organic matter mineralization in sediment of a coastal freshwater lake and response to salinization. Geochim Cosmochim Acta 2006;70:2836–55.

Carbonaro RF, Mahony JD, Walter AD, Halper EB, Di Toro DM. Experimental and modeling investigation of metal release from metal-spiked sediments. Environ Toxicol Chem 2005;24:3007–19.

Carroll S, O'Day PA, Esser B, Randall S. Speciation and fate of trace metals in estuarine sediments under reduced and oxidized conditions, seaplane lagoon, Alameda Naval Air Station (USA). Geochem Trans 2002;3:81–101.

Cline JD. Spectrophotometric determination of hydrogen sulfide in natural waters. Limnol Oceanogr 1969;14:454–8.

Davison W, Phillips N, Tabner BJ. Soluble iron sulfide species in natural waters: Reappraisal of their stoichiometry and stability constants. Aquat Sci 1999;61:23–43.

Davison W, Fones G, Harper M, Teasdale P, Zhang H. Dialysis, DET and DGT: in situ diffusional techniques for studying water, sediments and soils. In: Buffle J, Horvai G, editors. In situ chemical analysis in aquatic systems. Chichester: Wiley; 2000. p. 495–569.

Di Toro D, Mahony J, Hansen D, Scott K, Hicks M, Mayr S, et al. Toxicity of cadmium in sediments: the role of acid volatile sulfide. Environ Toxicol Chem 1990;9:1487–502.

Di Toro DM, Mahony JD, Hansen DJ, Berry WJ. A model of the oxidation of iron and cadmium sulfide in sediments. Environ Toxicol Chem 1996;15:2168–86.

Douglas GB, Adeney JA. Diagenetic cycling of trace elements in the bottom sediments of the Swan River Estuary, Western Australia. Appl Geochem 2000;15:551–66.

Dyrssen D, Kremling K. Increasing hydrogen sulfide concentration and trace metal behavior in the anoxic Baltic waters. Mar Chem 1990;30:193–204.

Gallon C, Tessier A, Gobeil C, Alfaro-De La Torre MC. Modeling diagenesis of lead in sediments of a Canadian Shield lake. Geochim Cosmochim Acta 2004;68:3531–45.

Holmer M, Storkholm P. Sulphate reduction and sulphur cycling in lake sediments: a review. Freshw Biol 2001;46:431–51.

Huerta-Diaz MA, Morse JW. A quantitative method for determination of trace metal concentrations in sedimentary pyrite. Mar Chem 1990;29:119–44.

Huerta-Diaz MA, Carignan R, Tessier A. Measurement of trace-metals associated with acid volatile sulfides and pyrite in organic freshwater sediments. Environ Sci Technol 1993;27:2367–72.

Huerta-Diaz MA, Tessier A, Carignan R. Geochemistry of trace metals associated with reduced sulfur in freshwater sediments. Appl Geochem 1998;13:213–33.

Hyacinthe C, Van Cappellen P. An authigenic iron phosphate phase in estuarine sediments: Composition, formation and chemical reactivity. Mar Chem 2004;91:227–51.

Jourabchi P, Van Cappellen P, Regnier P. Quantitative interpretation of ph distributions in aquatic sediments: a reaction–transport modeling approach. Am J Sci 2005;305:919–56.

Kay JT, Conklin MH, Fuller CC, O'Day PA. Processes of nickel and cobalt uptake by a manganese oxide forming sediment in Pinal Creek, globe mining district, Arizona. Environ Sci Technol 2001;35:4719–25.

Kostka JE, Luther GW. Partitioning and speciation of solid-phase iron in salt-marsh sediments. Geochim Cosmochim Acta 1994;58:1701–10.

Morse JW, Arakaki T. Adsorption and coprecipitation of divalent metals with mackinawite (FeS). Geochim Cosmochim Acta 1993;57:3635.

Morse JW, Luther GW. Chemical influences on trace metal–sulfide interactions in anoxic sediments. Geochim Cosmochim Acta 1999;63:3373–8.

Motelica-Heino M, Naylor C, Zhang H, Davison W. Simultaneous release of metals and sulfide in lacustrine sediment. Environ Sci Technol 2003;37:4374–81.

Naylor C, Davison W, Motelica-Heino M, van den Berg GA, van der Heijdt LM. Simultaneous release of sulfide with Fe, Mn, Ni and Zn in marine harbour sediment measured using a combined metal/sulfide DGT probe. Sci Total Environ 2004;328:275–86.

Paalman MAA, van der Weijden CH. Trace metals in suspended matter from the Rhine/Meuse Estuary. Neth J Sea Res 1992;29:311.

Perret D, Gaillard JF, Dominik J, Atteia O. The diversity of natural hydrous iron oxides. Environ Sci Technol 2000;34:3540–6.

Postma D, Jakobsen R. Redox zonation: equilibrium constraints on the Fe(III)/SO4-reduction interface. Geochim Cosmochim Acta 1996;60:3169–75.

Reinhold-Dudok van Heel HC, den Besten PJ. The relation between macroinvertebrate assemblages in the Rhine–Meuse Delta (The Netherlands) and sediment quality. Aquat Ecosyst Health Manag 1999;2:19–38.

Rickard D, Morse JW. Acid volatile sulfide (AVS). Mar Chem 2005;97:141–97.

Roden EE. Fe(III) oxide reactivity toward biological versus chemical reduction. Environ Sci Technol 2003;37:1319–24.

Sarazin G, Michard G, Prevot F. A rapid and accurate spectroscopic method for alkalinity measurements in sea water samples. Water Res 1999;33:290–4.

Slomp CP, Epping EHG, Helder W, van Raaphorst W. A key role for iron-bound phosphorus in authigenic apatite formation in North Atlantic continental platform sediments. J Mar Res 1996;54:1179–205.

Smit H, Smits R, van der Velde G, Coops H. Ecosystem responses in the Rhine–Meuse Delta during two decades after enclosure and steps toward estuary restoration. Estuaries 1997;20:504–20.

Smith SL, Jaffe PR. Modeling the transport and reaction of trace metals in water-saturated soils and sediments. Water Resour Res 1998;34:3135–47.

Taillefert M, MacGregor BJ, Gaillard JF, Lienemann CP, Perret D, Stahl DA. Evidence for a dynamic cycle between Mn and Co in the water column of a stratified lake. Environ Sci Technol 2002;36:468–76.

Tessier A, Fortin D, Belzile N, DeVitre RR, Leppard GG. Metal sorption to diagenetic iron and manganese oxyhydroxides and associated organic matter: Narrowing the gap between field and laboratory measurements. Geochim Cosmochim Acta 1996;60:387–404.

Thullner M, Van Cappellen P, Regnier P. Modeling the impact of microbial activity on redox dynamics in porous media. Geochim Cosmochim Acta 2005;69:5005.

Turner A, Millward GE, Le Roux SM. Significance of oxides and particulate organic matter in controlling trace metal partitioning in a contaminated estuary. Mar Chem 2004;88:179–92.

van den Berg GA, Loch JPG, van der Heijdt LM, Zwolsman JJG. Mobilisation of heavy metals in contaminated sediments in the River Meuse, The Netherlands. Water Air Soil Pollut 1999;116:567–86.

Wolthers M, Charlet L, van der Linde PR, Rickard D, van der Weijden CH. Surface chemistry of disordered mackinawite (FeS). Geochim Cosmochim Acta 2005;69:3469.

Zhang H, Davison W, Miller S, Tych W. In-situ high-resolution measurements of fluxes of Ni, Cu, Fe, and Mn and concentrations of Zn and Cd in porewaters by DGT. Geochim Cosmochim Acta 1995;59:4181–92.